

Fe-based high-temperature superconductivity: Impact of atomic defects in the electronic states

Yanina Fasano^{1, 2, 3}

¹ Instituto de Nanociencia y Nanotecnología, CNEA and CONICET, Nodo Bariloche, Avenida Bustillo 9500, 8400 Bariloche, Argentina

² Centro Atómico Bariloche and Instituto Balseiro,

CNEA and Universidad Nacional de Cuyo, Avenida Bustillo 9500, 8400 Bariloche, Argentina

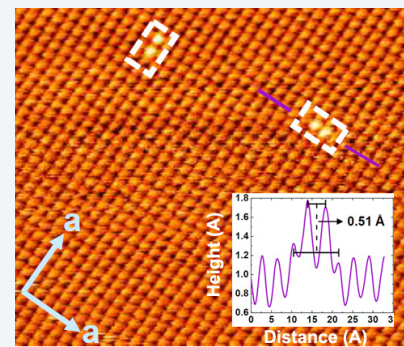
³ Leibniz Institute for Solid State and Materials Research, Helmholtzstraße 20, 01069 Dresden, Germany (Dated: January 19, 2023)

E-mail: yanina.fasano@cab.cnea.gov.ar

Abstract

A brief review on the impact of atomic defects in the electronic properties of Fe-based superconductors is hereby presented, focusing in particular on the FeSe family of superconductors. This family of compounds captured the attention of the scientific community during the last decade since its simple crystal structure seemed to be an advantage in understanding the microscopic mechanisms mediating high-temperature superconductivity in Fe-based superconductors. Now, more than 14 years of intense research around the world have elapsed since the discovery of the so-called iron age of superconductivity, and nevertheless it is still debated which is the origin of superconductivity in these compounds. One thing stands for certain in all the enquiries: There is a subtle interplay between defects or local variations in the crystal structure and the electronic states in Fe-based superconductors. This review presents an overview on the main contributions of the community in this interplay in the particular case of the FeSe family and provides a critical discussion on some of the points that still need to be studied in order to provide a thorough quantitative understanding of this issue.

Keywords: Fe-based superconductors; electronic states; atomic defects



I. Introduction

The first family of high-temperature superconductors was revealed back in 1986¹⁻³ and very rapidly several cuprate compounds with critical temperatures exceeding the boiling point of nitrogen were discovered.^{4,5} For 15 years subsequent to this discovery, these family of complex oxides of copper seemed to be the only high-temperature superconductors. However, 2008 witnessed the advent of the so-called iron-age of high temperature superconductivity.⁶ The Fe-based pnictides and chalcogenides are thus the second family of un conventional high-temperature superconductors that renewed the hopes on discovering materials with technically relevant critical temperatures. Superconductivity with a critical temperature of $T_c = 26$ K was first reported in the $\text{LaO}_{1-x}\text{F}_x\text{FeAs}$ and was followed by numerous reports in several members of the Fe-based superconductors family.⁷⁻¹¹ Within this family, iron chalcogenides, and particularly the 11 phase material FeSe,⁷ has attracted much attention due to its simple crystal structure of stacks of superconducting layers. Within these layers, a square/tetrahedral planar lattice of Fe cations are tetrahedrally coordinated with Se atoms located above and below the plane at a distance z_{Se} , see Fig. 1 (a). This compound is also considered as the prototype for studying the origin of unconventional super conductivity in the whole Fe-based superconductors family.¹²

FeSe is also special since it puzzles the identification of the microscopic mechanisms giving rise to high temperature superconductivity in the Fe-based family. Most of the compounds of this family develops a magnetic order apparently connected to the emergence of superconductivity.^{12,13} However, FeSe presents no static magnetic order at ambient pressure.^{13–15} This compound also undergoes a tetragonal-to-orthorhombic transition on cooling around $T_s \sim 90$ K¹⁶ without presenting any magnetic transition.^{17,18} This transition is also considered a nematic transition since the C4 symmetry of the crystal structure and of the electronic properties are both broken at T_s .¹⁹ In addition, applying pressure or doping FeSe with chalcogen atoms alters significantly the phase diagram²⁰ and enhances magnetic instability.²¹ Indeed, the idea that spin fluctuations have a relevant role in the superconducting pairing mechanism of Fe-based superconductors is suggested by spectroscopic information provided by scanning tunneling microscopy (STM).^{22–24} Then, in the paradigmatic material FeSe the crystal structure and electronic properties such as superconductivity and magnetism are tightly enmeshed.

In the quest for enhancing the T_c of Fe-based superconductors, FeSe provided valuable information. In its pristine form, FeSe has a T_c of 8 K, but it can be enhanced up to 37 K by applying hydrostatic pressure,^{25,26} or up to 30 K by intercalation of alkali metals between the layers.²⁷ For instance, Fig. 1 (b) shows the increase of T_c with hydrostatic pressure reported in Ref. 26. These enhanced critical temperatures in FeSe are within the largest values for binary superconducting compounds in general. In addition, there has been a considerable amount of work in many pnictogen and chalcogen systems in order to find a correlation between T_c and the Fe-anion height.²⁸ All these efforts revealed that there exists an optimum value of the Fe-anion height of ~ 1.38 Å that maximizes the T_c for many compounds of the Fe-based superconductors as shown in Fig. 1 (c) and discussed in detail in Ref. 28. Thus, the value of the Fe-anion height is a critical parameter in order to tune T_c .

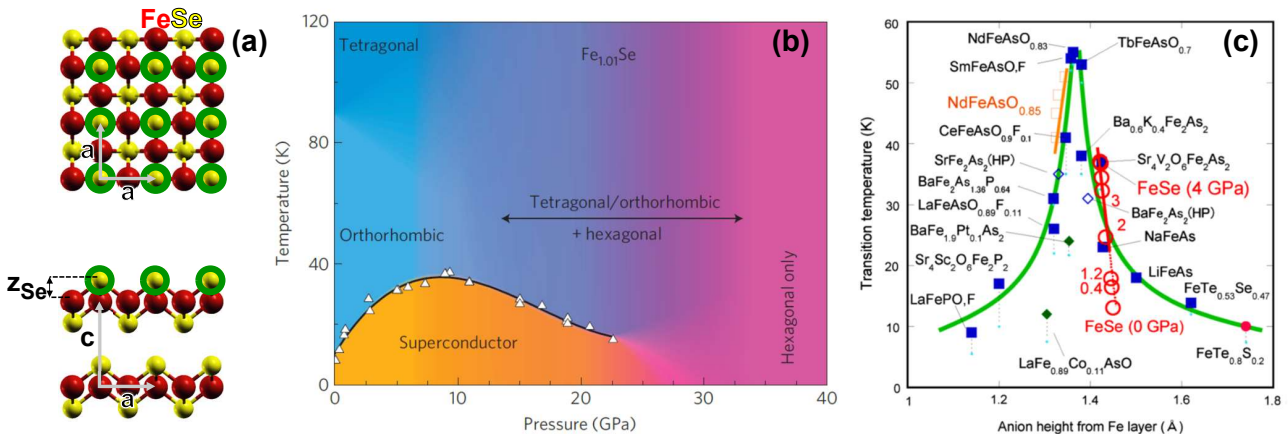


Figure 1. (a) Schematic representation of the FeSe crystal structure in the tetragonal phase at $T > 90$ K. The $a = 3.77$ Å and $c = 5.52$ Å unit cell vectors as well as the Fe-anion height z_{Se} are indicated. Reprinted from 43. (b) Evolution of the critical temperature (white points) and the electronic phase diagram of FeSe with hydrostatic pressure. The highest value of $T_c = 36.7$ K is reached at a pressure of 8.9 GPa. For no applied pressure the compound undergoes a tetragonal-to-orthorhombic transition on cooling through 90 K. Reprinted from 26. (c) Variation of T_c with the Fe-anion height for several compounds of the Fe-based superconductors family. Data for the paradigmatic FeSe compound are shown in open red circles and labelled with the value of the applied hydrostatic pressure between 0 and 4 GPa. Color points correspond to T_c values for several compounds as labelled. Full points are measured at ambient pressure whereas open points are measured at the optimal pressure (tiny diamonds) and at high pressures (open squares). Reprinted from 28.

In real samples, local crystal deformations and atomic scale defects are unavoidably present. If these deformations and defects entail local variations of z_{Se} , then a significant impact in the critical temperature and electronic states of the compounds is expected. In addition, the crystal structure deformations induced by introducing chemical pressure in the material by isovalently substituting Se with another chalcogen element²⁹ also affect the critical temperature of the compounds.²⁰ A remarkable example on how crystal structure and electronic properties are finely intertwined in FeSe is the important enhancement of T_c when growing strained mono layer films on top of SrTiO₃ substrates³⁰, or when coating the samples with K adatoms.³¹ Thus, understanding the impact of atomic-scale defects and deformations in the electronic structure of Fe-based superconductors is of key importance for assessing how critical is the occurrence of these features for the establishment of superconductivity in these compounds.

In addition, understanding their identity is fundamental to try to develop an engineering of superconducting/non-superconducting regions in Fe-based superconductors for nanoscale applied devices. Furthermore, a precise local control

of the location of atomic-scale defects would allow the tuning of electronic properties of the materials for applications as for instance achieved in other condensed matter systems such as in the case of dopants in semiconductors³² and silicon.³³ From a more general perspective, atomic defects in Fe based superconductors are determinant in the control of their critical temperature^{6,34} and the enhancement of their critical current by increasing vortex pinning.^{35,36} Local atomic defects in Fe-based superconductors can also be used as probes for testing the possible pairing symmetry in these compounds.³⁷

Here we review some of the most prominent experimental evidences on the impact of atomic-scale defects in the electronic properties of Fe-based superconductors focusing on compounds of the simplest FeSe family. Data available in the literature for this family is revisited and a recent experimental approach applied to obtain complementary atomic-scale and nanometer-thick bulk information on the topic is finally presented. Section II presents a critical discussion on the previous atomic-scale evidence from STM data in FeSe compounds. Section III overviews the findings obtained in an end-of-the-world research center on how the atomic-scale defects affect the bulk electronic core states by combining STM and XPS measurements. Finally, the Section IV is devoted to the conclusions and open questions on the topic with the aim of identifying the particular issues that deserve to be studied in order to better quantify how the unavoidable presence of atomic scale defects in Fe-based superconductors tailor its electronic properties and may eventually lead to locally or globally spoiling superconductivity in these compounds.

II. Previous atomic-scale evidence from STM data in FeSe

There is plenty of evidence obtained with scanning tunnelling microscopy (STM) that atomic-scale crystal structure modifications such as defects do play a role in the electronic and superconducting properties of materials.^{38,39} The scanning tunnelling microscope is a suitable tool to study these issues since it probes the electronic density of states in real space with atomic spatial resolution. In a STM experiment the spatially-mapped tunnel current is proportional to the convolution of the local density of states of the sample and the tip, and to an exponential multiplicative term that grows with decreasing the tip-sample distance.³⁸ Topographic images acquired either at constant height or current are proportional to the integration of the local density of states of the sample up to the regulation voltage as well as to the mentioned exponential factor,³⁸ and thus brighter features where the tunnel current is larger result from a region with a larger apparent height and/or a larger local density of states. Measuring a larger local density of states can arise from a local electronic inhomogeneity with an inherent larger value of this magnitude and/or from a protrusion of the local electronic clouds towards the STM tip that results in a smaller tip-sample distance.

One of the first works reporting on the impact of atomic defects in the superconducting properties of Fe based superconductors was published with the main aim of studying the thickness-dependence of the T_c of FeSe films grown by molecular beam epitaxy (MBE) on top of bilayer graphene substrates.⁴⁰ The authors find that T_c scales inversely with the film thickness and that a superconducting gap is detected in in-situ STM measurements for the thinnest studied film made of two c-axis unit cells of FeSe. The work presents a study on how the temperature of the substrate during the growing is determinant for the films being superconducting: Only when this temperature is larger than 420 C the films present a superconducting phase. Figure 2 shows examples of atomic-resolution STM topographies of non superconducting (a) and superconducting (b) FeSe films grown in bilayer graphene substrates kept at 390 and 450 C, respectively, during the MBE growing process. In these images each round-like brighter spot corresponds to an apical Se atom located above the Fe plane (atoms highlighted in green in Fig. 1). The films grown with a substrate temperature larger than 420 C present a depletion of the STM-measured tunneling conductance at low temperatures, even for films with a thickness $d = 2$ c-axis unit cells, see Fig. 2 (d). This tunneling conductance is proportional to the local density of states of the system and its depletion around zero bias is a manifestation of a finite superconducting gap that inhibits the tunneling of electrons from the sample to the tip since they are bounded in superconducting Cooper pairs. On increasing temperature this depletion fills in and disappears at the critical temperature T_c as expected for a superconducting material.

On addition to these findings on the optimization of the growing conditions for having superconducting very thin FeSe films, this work also presents evidence on the dramatic impact of dumbbell-type atomic defects on super conductivity. A dumbbell defect is observed as a brighter pair of contiguous Se atoms, as for instance clearly visible in the topography of the FeSe film shown in Fig. 2 (a). This type of defects was ubiquitously observed in subsequent works applying STM in FeSe films and crystals.^{29,37,41-43} The authors of this work do not investigate via first principle calculations on the nature of these defects, but they only speculate that they are associated to excess Se. Nevertheless, they show that the density of dumbbell defects can be controlled by the growing conditions of the film and by subsequent annealing at high temperatures. More importantly, they report that no depletion of the tunnelling conductance is detected for FeSe films presenting a concentration of dumbbell defects at the surface larger than 2.5 %. Further support to this statement is invoked from previous evidence obtained in thicker MBE-grown FeSe films within the same research group.¹⁹ Thus, in the case of very thin FeSe films super conductivity is spoiled on increasing the dumbbell defect concentration above a relatively low critical value.

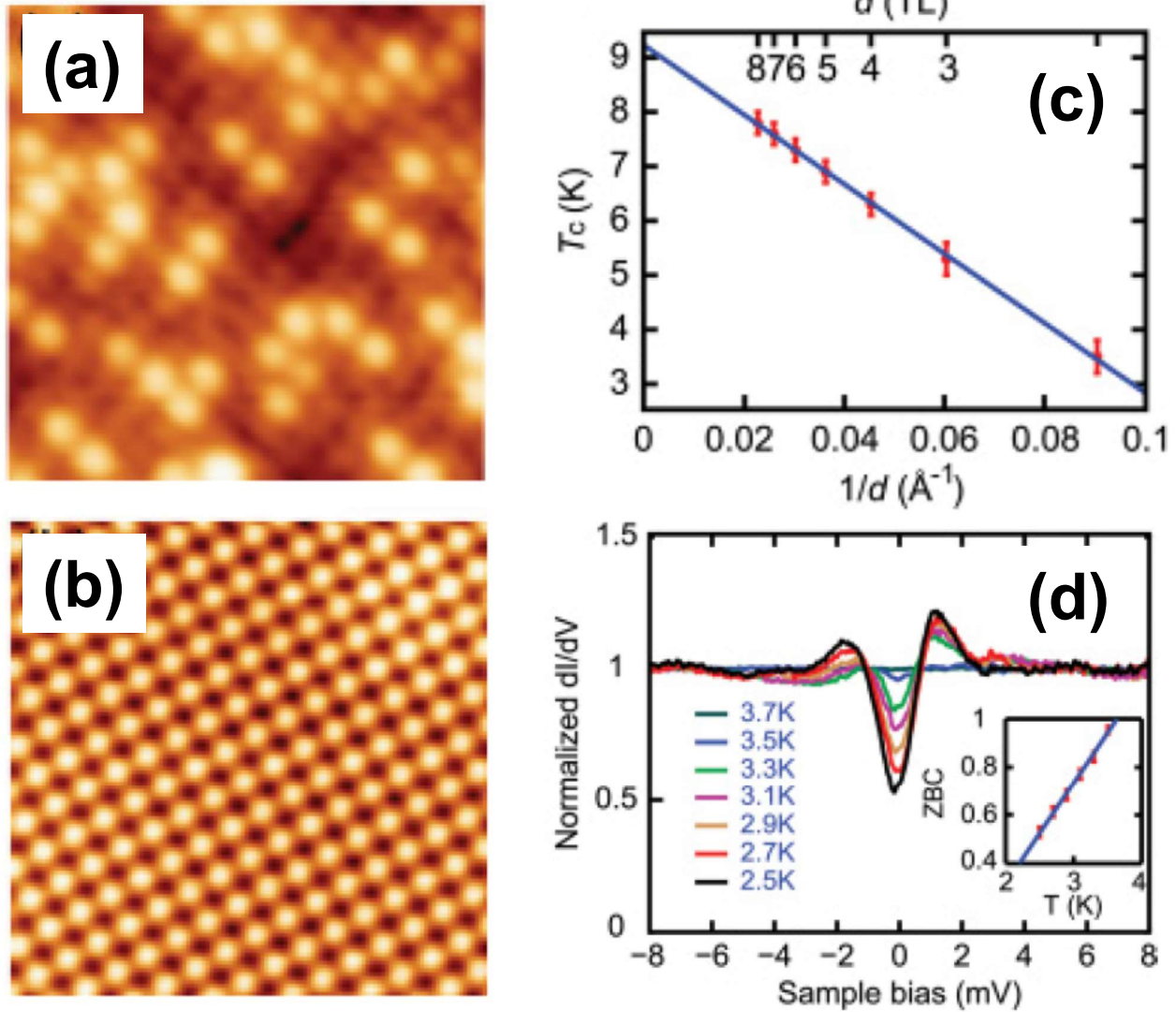


Figure 2. Atomic-resolution STM topographies of the surface of FeSe films grown by MBE at substrate temperatures of (a) 390 and (b) 450 C. The images survey an area of $5 \times 5 \text{ nm}^2$. Brighter atomic sites in (a) are associated to dumbbell defects in the crystal structure. (c) Inverse dependence of the critical temperature T_c with the film thickness d in units of c-axis unit cells (TL). (d) Normalized tunneling conductance curves at various temperatures for the thinnest film with $d = 2$ c-axis unit cells. The depletion of the tunnel conductance associated to the superconducting gap as well as the coherence peaks are observed up to 3.7, K. Insert: On increasing temperature within the superconducting phase the zero-bias conductance ZBC enhances. Reprinted from 40.

The nature of dumbbell defects was later studied in an experimental and theoretical work also studying MBE grown FeSe films.⁴¹ By conducting a STM and an exhaustive first-principles theoretical investigation of candidate defect configurations the authors of this work show that the dumbbell defects are induced by a vacancy in the site of Fe located below the two brighter Se atoms detected in topographies. By means of a density functional theory (DFT) analysis of the formation energies of different types of defects, this work shows that this is the most energetically favorable defect, overthrowing previous speculations^{19,40} of the dumbbell defects being associated to Se adsorbates or substitutions. In addition, they use STM to identify and estimate the defect concentration and compare the results with the DFT simulations in order to characterize the local electronic modifications entailed in these defects. Furthermore, this work studies experimentally and theoretically the previously reported removal and ordering of Fe vacancies (dumbbell defects) via annealing. Even though the authors resolve the chemical identity of these defects, they do not shed light on the question on how a large concentration of defects destroy superconductivity in FeSe films.

Figure 3 summarizes the main results obtained in the work of Huang *et al.*⁴¹ that are relevant for characterizing the chemical nature of dumbbell defects and some hints on their impact on the local electronic properties of superconducting FeSe. As in previous works,^{19,40} dumbbell defects in the studied FeSe films are observed as pairs of brighter Se atoms in atomic-resolution STM topographies of the surface. The studied FeSe films have thicknesses of a few *c*-axis unit cells and are grown by MBE on two different substrates, SiC and SrTiO₃. For example, Fig. 3 (a) shows a topographic image measured in the orthorhombic phase (84 K) of a few-layer-thick film grown on SiC. This as-grown surface presents a noticeable density of pairs of brighter Se atoms associated to dumbbell defects. These defects can be removed by annealing, as observed in Fig. 3 (b) that shows a topography of the same film presented in (a) after annealing at 450 C for 2.5 h. By performing nudged elastic band calculations and 2D random walk simulations the authors of this work explain this effect showing that during vacuum annealing the Fe vacancies can diffuse to the edge of the atomic terraces and thus in the main part of the terraces the dumbbell defect density is reduced. Since the Fe vacancy site can be located in a site where a pair of Se atoms at the top layer is aligned along the *a*-axis or else in a site such that the pair of Se atoms is aligned along the *b*-axis, see Fig. 1 (a), dumbbell defects appear aligned in both crystal directions, as indicated with orange and yellow lines in Fig. 3 (c).

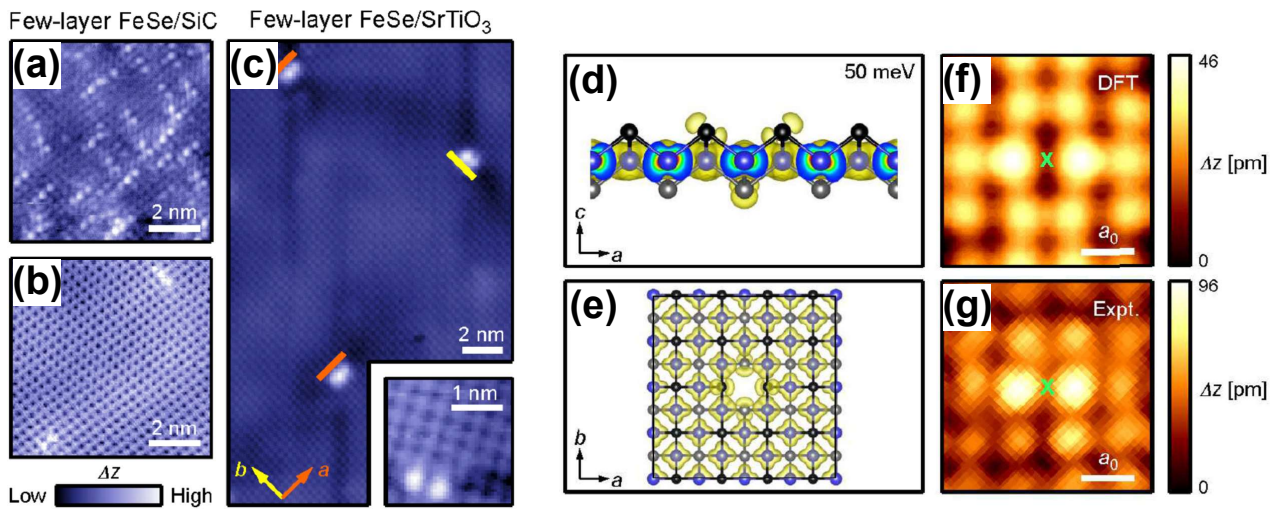


Figure 3. Dumbbell defects observed as pairs of brighter Se atoms in atomic-resolution STM topographies of the surface of FeSe films with thickness of few *c*-axis unit cells grown by MBE on different substrates. (a) Film grown on SiC measured at 84 K. (b) Topographic image obtained in the same film after annealing at 450 C during 2.5 h. (c) Film grown on SrTiO₃ and measured at ~ 6 K. Orange and yellow lines indicate the two possible orientations of dumbbell defects, parallel to the *a* and *b* unit cell vectors of the FeSe orthorhombic structure. (d) Charge density isosurface obtained with DFT simulations of bilayer FeSe in the *c* - *a* plane in the vicinity of a dumbbell defect induced by an Fe vacancy. Se atoms are shown in blue whereas Fe atoms are black. The electronic clouds associated to every atom are highlighted in yellow. The protrusion towards outside of the surface of the electronic clouds of the Se atoms adjacent to the Fe vacancy is evident. Image obtained integrating the density of states from the Fermi energy up to 50 meV. (e) Same calculation than in (d) but plotted in the *a* - *b* plane where the Fe vacancy producing the dumbbell defect is more clearly observed. (f) Topography obtained from the same simulations in the vicinity of the Fe vacancy indicated with a green cross. The neighbor Se atoms of the top surface show the brighter lobes producing the dumbbell signature. (g) Experimental STM topography of a single-layer FeSe film grown on SrTiO₃ in the neighborhood of a dumbbell defect. Reprinted from 41.

By modelling the local density of states of FeSe with DFT calculations the authors of this work⁴¹ provide important evidence on how the Fe vacancy perturbs the electronic cloud of the neighboring Se sites and thus produce the dumbbell signature imaged by STM. Figure 3 (d) depicts the charge density isosurface obtained with DFT simulations of a slab of FeSe in the *c* - *a* plane in the vicinity of a dumbbell defect. In this figure Se atoms are shown in blue whereas Fe atoms are black. The electronic clouds associated to every atom are highlighted in yellow. The Se atoms adjacent to the Fe vacancy present electronic clouds with a protrusion towards outside of the surface. Figure 3 (e) shows the result of the same calculation but plotted in the *a* - *b* plane where the Fe vacancy producing the dumbbell defect is more clearly observed. When measuring with an STM tip this spatial orientation of the electronic cloud of a pair of Se atoms will produce an enhancement of the tunnelling current since due to the protrusion of their orbitals the effective tip sample distance is smaller at atomic scale. This results in the pair of Se atoms adjacent to the Fe vacancy being observed as brighter than the rest. This explanation is further supported by the topographic image obtained from the same simulations in the vicinity

of the Fe vacancy indicated with a green cross in Fig. 3 (f). The neighbor Se atoms of the top surface show the brighter lobes producing the dumbbell signature. This simulated topography is in excellent agreement with the experimental STM topographies measured in the neighborhood of dumbbell defects observed in several FeSe films, as for example the one of Fig. 3 (g) corresponding to a single layer film grown on SrTiO₃. Whether the apical distance between the Se atoms and the Fe plane in the vicinity of a dumbbell defect is affected is not discussed in Ref. 41. In order to perform this study, DFT simulations should take into account the van der Waals interaction between adjacent Se and Fe planes as well as the correct magnetic order of Fe atoms in the FeSe material. These two issues were not considered in the work of Huang *et al.* Their consideration is of critical importance in order to have quantitative information on how atomic-scale dumbbell defects affect the local superconducting properties of the material.

Regarding this issue, phenomenological information was later provided by means of STM spectroscopy measurements with atomic resolution in the superconducting phase of FeSe single crystals.³⁷ In this work, the authors measure with atomic resolution the local density of states in the vicinity of dumbbell defects. In a superconducting material, the dI/dV tunnelling conductance measured by STM, proportional to the local density of states of the quasiparticle excitation spectrum, presents a depletion between energies $\pm\Delta$ around the Fermi level. This depletion is flanked by two coherence peaks located at energies around the superconducting gap for which the number of electrons tunnelling from the sample to the tip is maximized since this energy is around the value Δ required to break the superconducting Cooper pairs of electrons. Thus, the energy location of the coherence peaks in dI/dV STM curves is of the order of the superconducting gap. Conventional superconductors are expected to present symmetric peaks with the same height for occupied and empty sample states. Nevertheless, many materials present asymmetric dI/dV spectra produced by an asymmetry in the hole and electron bands of the materials,⁴⁴ as is for instance the case in FeSe according to angle/resolved photoemission spectroscopy data.²⁰ In the case of the spectra measured in FeSe crystals in Ref. 37, both away and close to the dumbbell defects the coherence peaks are asymmetric, see panels (c) and (d) of Fig. 4. In regions far away of the dumbbell defects, $\Delta \sim 2$ meV consistent with a $T_c = 0.46\Delta/k_B \sim 8$ K according to the BCS ratio for conventional superconductors. In contrast, on the sites of the Se atoms the peaks at 2 meV broaden and two extra peaks are detected at energies smaller than the superconducting gap, see Fig. 4 (d). These asymmetric peaks are rather sharp, sharper than what remains of the peaks at 2 meV, and are detected around 0.6 meV. The authors of this work state that these peaks located at smaller energies are bound states inside the superconducting gap. They perform DFT simulations in a slab of FeSe considering an Fe vacancy and show that the dumbbell defect is non-magnetic. Then they use this result to claim that the in-gap bound states emerging from a nonmagnetic defect-induced pair breaking suggest a sign-changing pairing state in FeSe.

Even though this can be concluded from the spin polarized DFT calculations presented in Ref. 37, as the same authors mention in the paper, they can not rule out the possibility that the in-gap coherence peaks in the vicinity of a dumbbell results from the spatial super imposition of the tunnelling response at the defect and the superconducting bulk. ON top of this possibility, I consider that the in-gap peaks can also have another origin due to technical issues of the STM measurements. In particular, even though the images of Fig. 4 have atomic resolution, since the image is not focused in the dumbbell region with high spatial resolution, and has a size larger than 20 times the area of the defect, it might be that the local dI/dV curves are collecting electrons tunnelling from the neighbor Se atomic sites that are not affected by the dumbbell defect. In order to discard this possibility, spectroscopic images with finer spatial resolution in the sub lattice spacing range are required. This information is not presented in Ref. 37. Thus, as the same authors mention, due to technical reasons of the STM technique, it is also quite likely that the extra in-gap peaks can be interpreted as due to a partial suppression of superconductivity at the defect site. This is consistent with coherence peaks located at smaller energies since that will yield a $\Delta \propto T_c$ smaller and then a local depletion of the superconducting critical temperature within the dumb bell. On top of STM data with finer and high spatial resolution in the vicinity of the dumbbell, more realistic DFT calculations than the ones presented in Refs. 37 and 41 are required to clarify this issue. In particular, these simulations should search for the possibility of the apical Se height being reduced in the vicinity of the dumbbell defect which will be in agreement with a reduction of T_c as ubiquitously observed in many Fe-based superconductors.²⁸

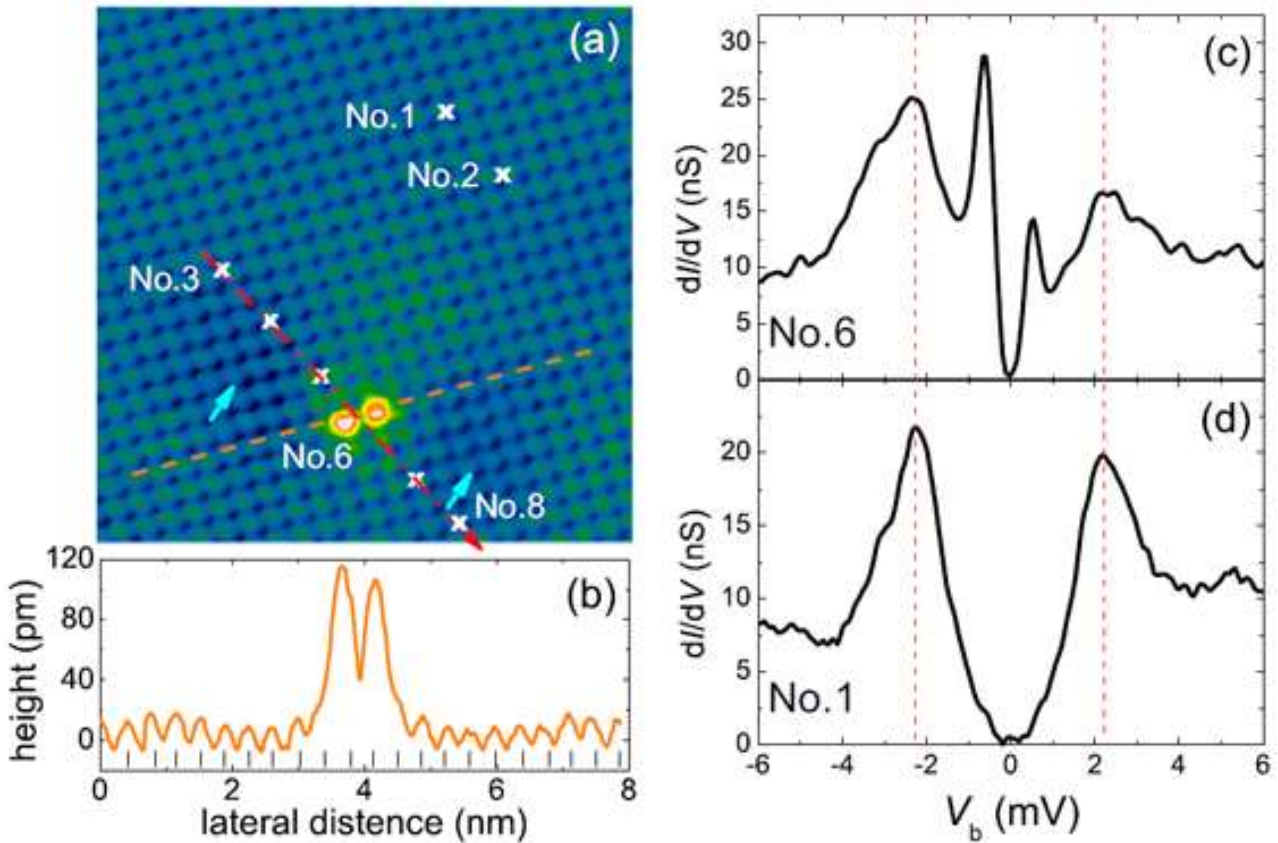


Figure 4. STM topographic and spectroscopic measurements in an FeSe single crystal performed in the superconducting phase at 350 mK. (a) Topographic image showing the Se atoms of the topmost layer in green. A dumbbell defect is imaged as brighter white Se atoms in the bottom-left part of the image. White crosses with numbers indicate the location where dI/dV tunnel spectra were measured. (b) Line-scan of apparent sample height measured along the red-dashed line going through the dumbbell defect in panel (a). (c) dI/dV vs. bias voltage V_b tunnel spectra measured close to the dumbbell defect (indicated with cross No. 6) and away from it at the location indicated with cross No. 1. The vertical lines in (c) and (d) indicate the energy location of the coherence peaks in the position away of the dumbbell defect at around 2 meV. Reprinted from 37.

III. Impact of dumbbell defects in the core electronic states of FeSe

After reviewing the more prominent results of the international community in the impact of atomic-scale defects in the electronic structure of Fe-based superconductors, it is rather clear that understanding this issue is of key importance for assessing how critical is the occurrence of these features for the establishment of superconductivity in these compounds. With the aim of studying this impact, a recent work combining real-space topographic imaging with STM and characterization of the electronic core states with X ray photoemission spectroscopy (XPS) brings new and relevant evidence on this issue.⁴³ This work, performed at the Centro Atómico Bariloche of Argentina, makes a qualitative connection between the occurrence of atomic-scale dumbbell defects imaged by means of STM and the spectral shape of electronic states revealed via XPS.

The study combines these two surface sensitive techniques to study high-quality single crystals⁴⁵ of $\text{FeSe}_{1-x}\text{S}_x$ with $T_c = 9.6$ K for $x = 0$ and 10 K for the $x \sim 0.03$ samples studied. Several structural studies in these crystals^{43,45} indicate that the samples do not show any detectable trace of spurious phases, an issue that is very relevant for a technique like XPS that is sensitive to the topmost layers of the sample but unlike STM collect information on a millimeter-size area of the sample and not locally. Transport data presented in this work for the temperature range in the vicinity of the tetragonal to-orthorhombic transition also provide evidence on the absence of any detectable spurious non-superconducting phases in the studied high-quality crystals.

Figure 5 show examples of STM topography images of the $\text{FeSe}_{1-x}\text{S}_x$ crystals studied in the tetragonal phase (normal state) of Ref. 43. The topmost Se atoms located above the top Fe plane and exposed by cleaving are shown as white

spots. These atoms are highlighted in green in the schematic crystal structure of Fig. 5 (e). Topographic images for pure and S-doped samples show a ubiquitous feature: Pairs of brighter Se atoms aligned in the *a* directions, see dashed-white frames in Figs. 5 (a) and (b). These brighter atoms are dumbbell defects and as in previous reports are observed as higher atomic peaks in traces of profile height, see Fig. 5 (c). Statistics in several areas of different samples show that the distribution of dumbbell defects is quite diluted, representing 4.2(0.6) and 3.8(0.6) % of the STM-imaged Se atoms in the pure and S-doped samples, respectively. Fig. 5 (f) schematically recalls the modifications on the electronic clouds of Se and Fe atoms surrounding a dumbbell defect predicted by DFT simulations:⁴¹ the 2 Se atoms located above the Fe plane and imaged as brighter by STM (orange) show electronic clouds protruding out of the surface of the sample, and the electronic clouds of the 2 Se atoms located below the plane (magenta) and the 4 first-neighbor Fe atoms (turquoise) are asymmetric. The schematics of the charge density isosurfaces in the plane, see right part of Fig. 5 (f), highlights the asymmetry in the shape of the electronic clouds of these 8 atoms with respect to the symmetric ones expected for atoms located further away from the defect (4 Fe atoms with red clouds). As previously discussed, these protrusions of the electronic cloud result in an apparent larger height (brighter spots) of the Se atoms entailed in the dumbbell defect. It is important to point out that although the density of dumbbell defects imaged by STM is small, this technique only reveals defects at the sample surface and such defects can certainly occur in every FeSe plane of the crystal. For dumbbell defects located in the bulk of the sample instead than in the surface, it may be quite likely that the protrusion and the asymmetry in the charge distribution has a lesser magnitude. This is something that deserves further theoretical investigation by means of DFT simulations of defects in a bulk or at least a trilayer sample instead of in a monolayer as studied in Ref. 41. These simulations are probably not yet feasible with state-of-the-art simulation clusters. Even though the magnitude of the modifications of the electronic clouds of dumbbell defects located in the bulk can not be quantified yet, the Se atoms with altered electronic environment surrounding the dumbbell defects surely have a small but maybe noticeable impact in the bulk electronic properties of the samples.

This work⁴³ shows that for S-doped samples, another prominent topographic feature is also imaged in several locations. This feature consists in a local depletion of the apparent sample height associated to darker chalcogen atoms. Height profiles along these features indicate that in the darker areas there is a height depletion of roughly 25 % with respect to neighbor Se atoms, see for example Fig. 5 (d). These features are not detected in measurements in pure FeSe crystals from different origin.^{29,41-43} These defects were also observed in STM topographies of S-doped crystals with an occurrence that grows with the S concentration.²⁹ Given that S has a smaller atomic radius than Se, it can be assumed that S atoms are imaged by STM as these darker features entailing a local height depletion.⁴³ Irrespective of the nature of the defects introduced by S doping, these results indicate that crystal disorder is more important in S-doped samples than in pure ones.

The connection between these atomic defects and the electronic core states is performed in Ref. 43 by means of detailed fits of the peaks detected in XPS spectra. XPS measurements provide information on the energy spectrum of the core levels of the different elements composing the material. As discussed in Ref. 43, in the XPS spectra measured in the studied FeSe_{1-x}S_x crystals the Fe and Se contributions are detected at energies close to the ones corresponding to the tabulated peaks for the different core levels for the pure elements.⁴⁶ The S peaks are not clearly observed in the XPS spectra since they come from a small amount of S and are maybe hindered by the superimposition with the Se 3p peaks detected at closer energies than expected for S 2p, and also present a photoemission cross section 3 times smaller than those Se peaks. In addition, Ref. 43 discusses on the importance of analyzing XPS spectra of samples cleaved in-situ under UHV conditions since else extra peaks and deformations of peaks associated to the Fe levels are observed due probably to the oxidation of the topmost layer of the sample if not cleaved in-situ. This was also pointed out in a more recent paper studying ageing effects in air-cleaved FeSe crystals.⁴⁷

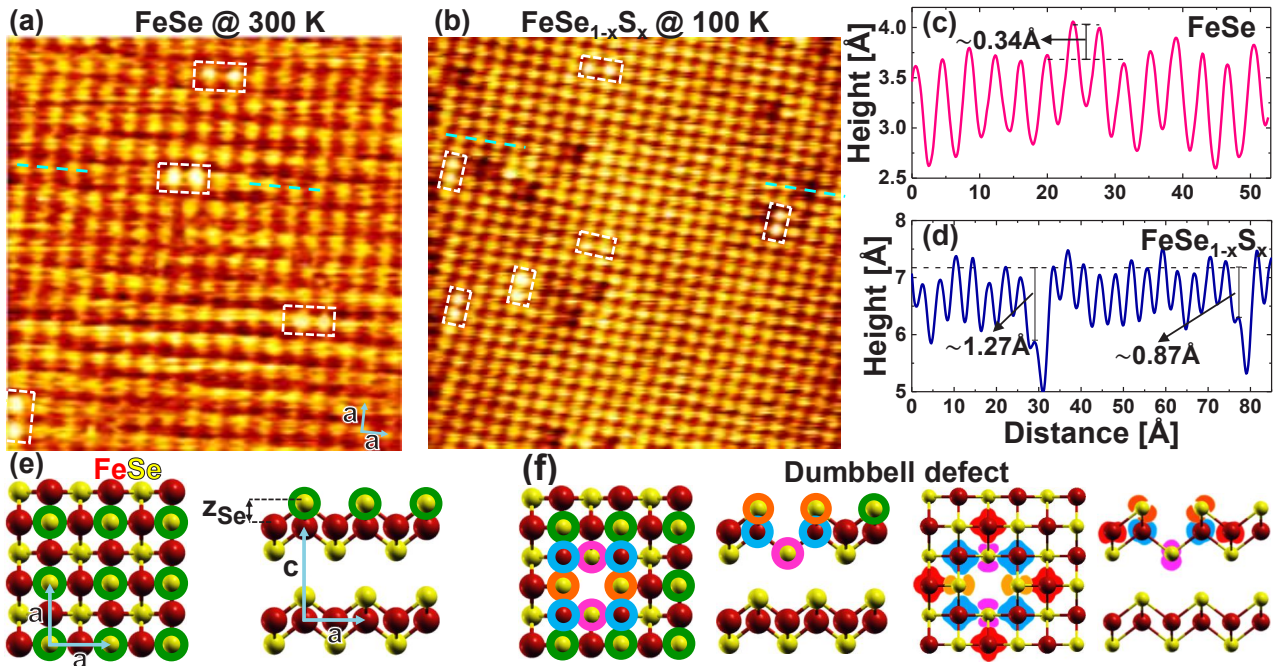


Figure 5. STM topography images and crystal structure of $\text{FeSe}_{1-x}\text{S}_x$ in the high-temperature tetragonal phase. (a) Topography of a single crystal with $x = 0$ where the exposed Se atoms are observed as bright spots. Dumbbell defects (see white dashed frames) are observed as two bright Se atoms oriented along the a -axis directions. (b) Topography of a crystal with $x \sim 0.03$ where local depletions of the sample height (darker chalcogen atoms) are presumably generated by smaller S dopant atoms. Dumbbell defects are also indicated with dashed-white frames. (c) Height-profile in FeSe along the trace indicated (partially) with a turquoise dashed line in panel (a) where a dumbbell defect is evident. (d) Height-profile in the S-doped crystal along the trace indicated with the turquoise line in panel (b). Local minima in the surface height are detected in the darker features. (e) Schematic representation of the FeSe crystal structure in the tetragonal phase with the measured $a = 3.77 \text{ \AA}$ and $c = 5.52 \text{ \AA}$ unit cell vectors indicated. When cleaving the samples to perform STM measurements, the Se atoms located above the top Fe plane are imaged (highlighted in green). (f) Schematic of a dumbbell defect associated with an Fe vacancy: Atomic positions (left) and charge density isosurfaces (right) of the atoms entailed in the defect. The atomic clouds of the neighbouring Se and Fe atoms are schematically reproduced from the DFT calculations of Ref.⁴¹. Reprinted from 43.

Figure 6 shows the most intense Se peaks of the XPS spectra reported in Ref. 43, the Se 3d doublet with two broad peaks centered at approximately 54 and 55 meV of binding energy for both the pure and S-doped samples. The study focus on the details of the XPS spectra in this energy range to ascertain both, if there is a surface contribution, and to describe the electronic states via fits of the data. Panel (a) of this figure presents the XPS spectra obtained for pure FeSe samples for two different detection angles for the photoemitted electrons. The shape of the measured spectra is almost independent of the detection angle within the noise level, implying that the measured spectra are not affected by possible surface states and are representative of the electronic levels in the bulk of a nanometer-thick top layer as probed by XPS. Panels (b) and (c) present data (color dots) measured in pure and S-doped samples, respectively. The spectral shape in this energy range for both types of samples are alike. Both present two sharp peaks corresponding to the Se $3d_{5/2}$ and $3d_{3/2}$ core levels and a broad peak around 53 eV associated with the Fe $3p_{3/2}$ and Fe $3p_{1/2}$ core levels are observed as a shoulder in the low-energy flank of the Se 3d peaks. The authors of this work fit these spectra considering: (a) Shirley background associated to the photoemission process of secondary electrons (black dashed line), (b) a pair of Voigt-like peaks for the Fe 3p doublet (full red lines), (c) two pairs of Voigt-like peaks for the Se 3d doublet (full green and magenta lines). The authors stress that it is compulsory to consider two pairs of Se 3d spin-orbit doublets, instead of one, in order to properly fit the data. In this fitting procedure, the corresponding spin-orbit splitting and statistical intensity ratios theoretically expected for both peaks of the doublet were left fixed, while the energy location of the pairs of peaks are allowed to vary. The main component corresponding to the green spin-orbit doublet is centered at exactly the same energies where the peaks are detected in the experimental spectra. This component represents 86 % (85 %) of the area under the curve of the Se 3d peaks fit in pure (S-doped) samples. The second contribution (magenta lines) is shifted 0.64 eV towards larger binding energies with respect to the experimentally detected peaks. The consideration of these minor contribution with an area under the curve of 14 % (15 %) is compulsory in order to properly fit the data in both, pure and S-doped FeSe samples.

The need of considering a second contribution to the Se 3d levels in order to properly fit the XPS data in both pure and S-doped samples indicates that a significant amount of Se atoms, roughly 14 %, has a different electronic environment than the rest of Se atoms. Since curves obtained in measurements performed at different detection angles are rather coincident, the authors rule out the origin of this second component on a surface associated state.⁴³ Based on a detailed analysis of X-ray, XPS and resistivity data that show no detectable traces of spurious phases⁴⁸ the authors rule out the possibility of this second component coming from intergrowths in the samples. The second component is thus only associated with local variations of charge transfer that occur in the nanometer-thick bulk of the samples probed by XPS.

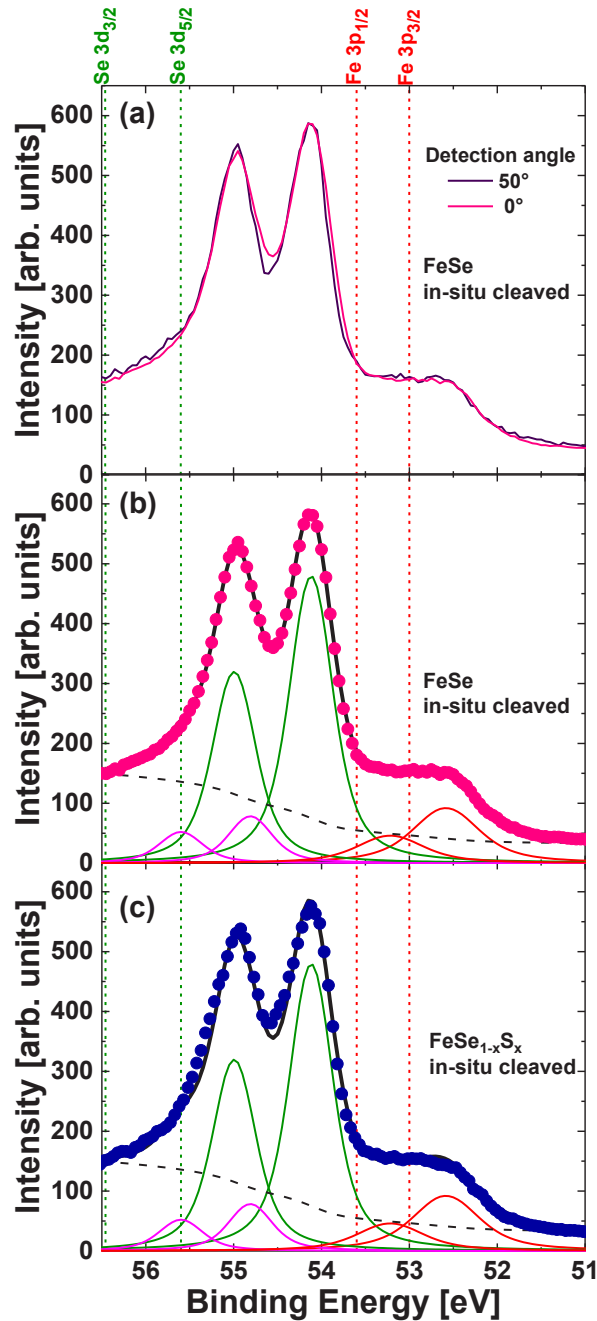


Figure 6. (a) XPS spectra in the energy region of the Se 3d and Fe3p peaks for a pure FeSe sample. Measurements performed at two different detection angles of photoemitted electrons. (b) Pink points: same data than in panel (a) for a detection angle of 0° (normal incidence). Full black line: Fit of the experimental data with a convolution of doublets of Voigt-like peaks after subtraction of a Shirley background (see black dashed line). The broad peak observed around 53 eV associated to the Fe 3p core levels is fitted with a spin-orbit doublet (see red lines). Two pairs of peaks shown with green and magenta lines come from a principal and a minor doublet contribution associated with the Se 3d core levels. (c) Same analysis than in panel (b) for the XPS spectra measured in the S-doped crystal at normal incidence. In all panels dashed vertical lines correspond to the tabulated values for the core level energies in the pure elements. Reprinted from 43.

Recalling that the atomic resolution images of $\text{FeSe}_{1-x}\text{S}_x$ shown in Fig. 5 as well as previous works in films and crystals of FeSe ^{29,41,42} present Fe vacancy induced dumbbell defects, the authors of Ref. 43 propose the second component in XPS spectra comes from the Se atoms with electronic clouds modified by the Fe vacancy at the dumbbell. Indeed, according to the DFT calculations of Huang *et al.*⁴¹, every dumbbell defect entails changes in the electronic environment of the 4 Se atoms surrounding the Fe vacancy. The experimentally detected density of Se atoms participating in dumbbell defects of roughly 3 %, and the area under the curve of the second Se 3d component in the XPS spectra, are roughly the same for pure and S-doped FeSe samples. This finding points on the second XPS component having the same electronic origin in both types of samples. In addition, the energy location of the doublet of the second component is at larger binding energies than the main component, a fact that is in agreement with the second component coming from a minority of Se atoms having an electronic environment with less charge produced by the lacking Fe atom at the dumbbell. Therefore, by combining local topographic imaging techniques and nanometer-thick bulk electronic measurements, this work⁴³ probes that in the Fe-based superconductor $\text{FeSe}_{1-x}\text{S}_x$ dumbbell-type atomic defects have an important effect on the electronic properties of the compounds.

IV. Summary and perspective

In conclusion, the experimental and theoretical works discussed in the previous two sections show that STM revealed local atomic-scale defects in the crystal structure of the simplest Fe-based superconductor have a noticeable impact in the electronic properties of the material. This effect is evidenced in the superconducting phase of the material^{19,37} as well as in the normal state phase,^{40,41,43} irrespective of the samples being crystals or few-layer thick films. A recent work goes further on this qualitative assertion and quantifies the impact of atomic scale defects in the core electronic states measured by XPS.⁴³ The authors show that a minor second component in the Se 3d doublet is compulsory to properly fit the spectral shape of XPS data. Since the area under the curve of this component is small and its energy location goes towards larger binding energies, implying a loss of charge in the Se induced by the Fe vacancy associated to the dumbbell defects, the authors propose that the second component is associated with the modification of the electronic cloud of the minority of Se atoms surrounding these defects.

Yet, several questions remain open as to completely settle the issue on the details of this interplay. For instance, the question on whether the height of the apical Se atoms neighbouring the dumbbell defect is affected by the Fe vacancy is very relevant. As mentioned in the introduction, most of the compounds of the broad Fe based superconductors family presents an optimal value of its critical temperature for a given value of this apical height.²⁸ This issue is particularly relevant since in the case of few-layer-thick FeSe films when dumbbell defects proliferate above a relatively small amount,⁴⁰ superconductivity is spoiled. Thus, more insight in the impact of atomic scale defects in the superconducting proper ties will be gained by performing DFT simulations that search for possible changes in the apical height of the Se atoms surrounding the dumbbell defects. Also, a careful study on this issue on increasing the defects density will allow to have an idea on the details on how super conductivity might be degraded in the FeSe compound. These simulations consume an extremely large computational time and are not affordable by regular simulation clusters, but certainly new studies would point in that direction in the future.

In addition, another issue that deserves further investigation to have a better quantitative understanding of the impact of dumbbell defects in FeSe is to correlate the area under the curve of the second component of the Se 3d levels and the amount of Se atoms that have a modified electronic cloud in the vicinity of the defects. Regarding this point, I would like to stress that it is possible that the Fe vacancy of a dumbbell affects the orbitals of more than the 4 Se surrounding atoms as proposed by Huang *et al.* Further DFT calculations appropriately considering the van der Waals intra and inter-layers interaction, and the stripe-antiferromagnetic magnetic state of the Fe atoms in this compound⁴⁹ are important to quantitatively assess the possibility of the electronic cloud of more than 4 Se atoms being affected by the Fe vacancy producing the dumbbell defect. The consideration of these two important issues in DFT simulations would also give more realistic information on the possible modification of the Se apical height around the dumbbell defects discussed above. In addition, further all-electron calculations are required in order to connect the information obtained with experimental STM imaging and first principle simulations as the DFT ones discussed here, with the shifting of a second component towards larger binding energies.

Ultimately, all the results presented in this review as well as the open questions highlight the impact of atomic defects in the binding energy and spectral shape of the core levels in $\text{FeSe}_{1-x}\text{S}_x$. The experimental and theoretical results discussed here in this family of compounds are just a notable example of the subtle interplay between the crystal structure and the electronic states in Fe-based superconductors in general.

Acknowledgments

I thank J. Aragón Sánchez, G. L. Nieva, M. L. Amigó, E. Gayone E. Martínez and C. Ventura for insightful discussions. Work supported by the Argentinean ANPCyT through grants PICT 2017-2182 and 2018-1533, by Con ictet through grant PIP 2021-1848 and by the Universidad Nacional de Cuyo research grants 06/C566 and 06/C575. The author also acknowledges funding from the Alexander von Humboldt Foundation of Germany through the Georg Forster Research Award.

References

- [1] Bednorz, J G and Müller, K A, *Z. für Physik B - Condensed Matter* 64, 189 (1986).
- [2] Chu, P. C. W, *Proc. Nat. Acad. Sciences* 84, 4681 (1987).
- [3] Takagi H, Uchida S, Kitazawa K and Tanaka S, *Jpn. J. Appl. Phys.* 26, 123 (1987).
- [4] Ginzburg V L, *Soviet Physics Uspekhi* 34, 283 (1991).
- [5] Chu P C W, *Scientific American*, 162 (1995).
- [6] Kamihara Y, Watanabe T, Hirano M. and Hosono, H, *J. Am. Chem. Soc.* 130, 3296 (2008).
- [7] Hsu F C, *et al.*, *Proc. Nat. Acad. Sciences* 105, 38 (2008).
- [8] Rotter M, Tegel M and Johrendt M, *Phys. Rev. Lett.* 101, 107006 (2008).
- [9] Tapp J H, Tang Z, Lv B, Sasmal K, Lorenz B, Chu P C W, Guloy A M, *Phys. Rev. B* 78, 060505 (2008).
- [10] Pitcher M J, Parker D R, Adamson P, Herkelrath S J C, Boothroyd A T, Ibberson R M, Brunelli M and Clarke S J, *Chem. Commun.* 45, 5918 (2008).
- [11] Wang X C, Liu Q Q, Lv Y X, Gao W B, Yang L X, Yu R C, Li F Y and Jin C Q, *Solid State Commun.* 148, 538 (2008).
- [12] Norman M R, *Physics* 1, 21 (2008).
- [13] Büchner B and Hess C, *Nature Materials* 8, 615 (2009).
- [14] Bohmer A E and Kreisel A, *J. Phys. Condens. Matter* 30, 023001 (2018).
- [15] Chen T, Yi M and Dai P, *Frontiers Phys.* 8, 00314 (2020).
- [16] Margadonna S, Takabayashi Y, McDonald M T, Kasperkiewicz K, Mizuguchi Y, Takano Y, Fitch A N, Suarde E and Prassides K, *Chem. Comm.* 43, 5607 (2008).
- [17] McQueen T M, Huang Q, Ksenofontov V, Felser C, Xu Q, Zandbergen H, Hor Y S, Allred J, Williams A J, Qu D, Checkelsky J, Ong N P and Cava R J, *Phys. Rev. B* 79, 014522 (2009).
- [18] Bendele M, Amato A, Conder K, Elender M, Keller H, Klauss H-H, Luetkens H, Pomjakushina M, Raselli A and Khasanov R, *Phys. Rev. Lett.* 104, 087003 (2010).
- [19] Song C-L *et al.*, *Science* 332, 1410 (2011).
- [20] Watson M D, Kim T K, Haghighirad A A, Blake S F, Davies N R, Hoesch M, Wolf T and Coldea A I, *Phys. Rev. B* 92, 121108 (2015).
- [21] Imai T, Ahilan K, Ning F L, McQueen T M and Cava R J, *Phys. Rev. Lett.* 102, 177005 (2009).
- [22] Fasano Y, Maggio-Aprile I, Zhigadlo N D, Katrych S, Karpinski J and Fischer Ø, *Phys. Rev. Lett.* 105, 167005 (2010).
- [23] Hoffman J E, *Rep. Prog. Phys.* 74, 124513 (2011).

- [24] Chi S, Grothe S, Liang R, Dosanjh P, Hardy W N, Burke S A, Bonn D A, and Penneç A, *Phys. Rev. Lett.* 109, 087002 (2012).
- [25] Margadonna S, Takabayashi Y, Ohishi Y, Mizuguchi Y, Takano Y, Kagayama T, Nakagawa T, Takata M and Prasad M, *Phys. Rev. B* 80, 064506 (2009).
- [26] Medvedev S, McQueen T M, Troyan I A, Palasyuk T, Eremets M I, Cava R J, Naghavi S, Casper F, Ksenofontov V, Wortmann G and Felser C, *Nature Materials* 8, 630 (2009).
- [27] Krzton-Maziopa A, Svitlyk V, Pomjakushina E, Puzniak R and Conder K, *J. Phys.: Condens. Matter* 28, 293002 (2016).
- [28] Mizuguchi Y, Hara Y, Deguchi K, Tsuda S, Yamaguchi T, Takeda K, Kotegawa H, Tou H, and Takano Y, *Supercond. Sci. Technol.* 23, 054013 (2010).
- [29] Hanaguri T, Iwaya K, Kohsaka Y, Machida T, Watashige T, Kasahara K, Shibauchi T and Matsuda Y, *Sci. Adv.* 4, eaar6419 (2018).
- [30] Ge J-F, Liu Z-H, Liu C, Gao C-L, Qian D, Xue Q-K, Liu Y and Jia J-F, *Nat. Mat.* 14 285 (2014).
- [31] Miyata Y, Nakayama K, Sugawara K, Sato T and Takahashi T, *Nat. Mat.* 14 775 (2015).
- [32] Kitchen D, Richardella A, Tang J-M, Flatté M E, Yazdani A, *Nature* 442, 436 (2006).
- [33] Weber B *et al.*, *Science* 335, 64 (2012).
- [34] Yeh K-W *et al.*, *Eur. Phys. Lett.* 84, 37002 (2008).
- [35] Yin Y, Zech M, Williams T L, Wang X F, Wu G, Chen X H, Hoffman J. E., *Phys. Rev. Lett.* 102, 097002 (2009).
- [36] Demirdiř S, van der Beek C J, Fasano Y, Cejas Bolecek N R, Pastoriza H, Colson D, Rullier-Albenque F, *Phys. Rev. B* 84, 094517 (2011).
- [37] Jiao L, Rößler S, Koz C, Schwarz U, Kasinathan D, Rößler U K, Wirth S, *Phys. Rev. B* 96, 094504 (2017).
- [38] Fischer Ø, Kugler M, Maggio-Aprile I, Berthod C, Renner Ch, *Rev. Mod. Phys.* 79, 353 (2007).
- [39] Jenkins N, Fasano Y, Berthod C, Maggio-Aprile I, Piriou A, Giannini E, Hoogenboom B W, Hess C, Cren T, Fischer Ø, *Phys. Rev. Lett.* 103, 227001 (2009).
- [40] Song C-L, Wang Y-L, Jiang Y-P, Li Z, Wang L, He K, Chen X, Ma X-C and Xue Q-K, *Phys. Rev. B* 84, 020503 (2011).
- [41] Huang D, Webb T A, Song C-L, Chang C-Z, Moodera J S, Kaxiras E and Hoffman J E, *Nano Lett.* 16, 4224 (2016).
- [42] Putilov A V, Di Giorgio C, Vadimov V L, Trainer D J, Lechner E M, Curtis J L, Abdel-Hafiez M, Volkova O S, Vasiliev A N, Chareev D A, Karapetrov G, Koshelev A E, Aladyskhin A Y, Mel'nikov A S, Iavarone M, *Phys. Rev. B* 99, 144514 (2019).
- [43] Aragón Sánchez J, Amigó M L, Belussi C H, Ale Crivillero M V, Suárez S, Guimpel J, Nieva G, Gayone J E, Fasano Y, *J. Phys. Mater.* 5, 044008 (2022).
- [44] Berthod C, Fasano Y, Maggio-Aprile I, Piriou A, Giannini E, Levy de Castro G, Fischer Ø, *Phys. Rev. B* 88, 014528 (2013).
- [45] Amigó M L, Ale Crivillero V, Franco D G, and Nieva G, *Journal of Phys.: Conf. Series* 568, 022005 (2014).
- [46] Moulder J F, Stickle W F, Sobol P E and Bomben K D, *Handbook of X-Ray Photoelectron Spectroscopy*, Minnesota: Perkin-Elmer Corporation (1992).
- [47] Lanoël L, Rozas G, Bruchhausen A E, Amigó M L, Ale Crivillero M V, Hofer J A, Villafuerte M, Bridoux G, Bengió S, Nieva G, *Phys. Rev. B* 106, 214507 (2022).

[48] Yamasaki A *et al.*, Phys. Rev. B 82, 184511 (2010).

[49] Lochner F, Eremin I M, Hickel T and Neugebauer J, Phys. Rev. B 103, 054506 (2021).

Bio



Yanina Fasano

Yanina Fasano performs research in the field of experimental condensed matter at low temperatures, focusing on superconductivity and vortex matter studied by means of spectroscopic techniques with

atomic resolution. She received her PhD in Physics from the Instituto Balseiro at Bariloche, Argentina, in 2003. After a postdoctoral appointment at the University of

Geneva, Switzerland, she joined the Low Temperatures Lab at the Centro Atómico Bariloche of the Atomic National Commission as a tenured researcher of Conicet. In 2021 she became assistant professor at the Instituto Balseiro. She received the Houssay prize of the Ministry of Science, Technology and Innovation of Argentina in 2022 and was honored with the Georg Forster Research Prize from the Alexander von Humboldt Foundation in 2021.